Novel approach to quantitative spatial gene expression uncovers cryptic evolution in the developing *Drosophila* eye

Sammi Ali[1*], Sarah A. Signor[1*+], Konstantin Kozlov[2], Sergey V. Nuzhdin[1,2]

[1]Molecular and Computational Biology, University of Southern California, Los Angeles, California, 90089 USA

[2]Department of Applied Mathematics, St. Petersburg State Polytechnic University, St. Petersburg, 195251, Russia

*Co-first author

[+]Corresponding author: 1050 Childs Way, Ray R. Irani Hall,
Molecular and Computational Biology
University of Southern California
Los Angeles, 90089
ssignor@usc.edu
Phone 213-740-3065

ABSTRACT

Robustness in development allows for the accumulation of cryptic variation, and this largely neutral variation is potentially important for both evolution and complex disease phenotypes. However, it has generally only been investigated as variation in the response to large genetic perturbations. Here we use newly developed methods to quantify spatial gene expression patterns during development of the *Drosophila* eye disc, and uncover cryptic variation in wildtype developmental systems. We focus on four conserved morphogens, *hairy*, *atonal*, *hedgehog*, and *Delta*, that are involved in specifying ommatidia in the developing eye. We find abundant cryptic variation within and between species, genotypes, and sexes, as well as cryptic variation in the regulatory logic between *atonal* and *hairy* and their regulators, *Delta* and *hedgehog*. This work paves the way for a synthesis between population and quantitative genetic approaches with that of developmental biology.

Introduction

Natural genetic variation within populations has long been the purview of evolutionary and population geneticists, while developmental biologists focus on the effect of large mutations in otherwise isogenic backgrounds (Paaby and Gibson 2016). This dearth of work on developmental variation in wildtype genetic backgrounds is in part because developmental approaches have long been restricted to data that is at best semi-quantitative (i.e. *in situ* hybridization, antibody staining). Indeed, gene expression studies are generally spatial or quantitative, but not both. Without quantitative replication, there can be no rigorous statistical testing when developmental processes are compared among conditions, including health versus disease. This is especially important given the potential for cryptic variation to result in disease phenotypes, for example the complex disease phenotypes seen in humans after their recent, rapid change in lifestyle (Gibson and Reed 2008; Gibson 2009; Felix 2012; Ward and Kellis 2012; Hu et al. 2016). Here we use hybridization chain reaction (HCR) to bridge this gap between developmental and quantitative or population genetics by quantitatively measuring spatial gene expression in multiple genotypes from two sexes of two species (*Drosophila melanogaster* and *D. simulans*). This is essentially the first 'population genetics of development' as we are able to evaluate wild type differences in spatial and quantitative gene expression at the level of genotype, species and sex. This includes the ability to multiplex four genes, as more commonly co-expression is inferred across samples. We use this enormous developmental dataset to focus on the well-known morphogens driving ommatidia specification in *Drosophila* (Li et al. 1995; Raj et al. 2008; Tsachaki and Sprecher 2011; Atkins et al. 2013; Shah et al. 2016).

The *Drosophila* eye is formed from an imaginal disc, which is initially patterned by a wave of differentiation marked by a visible indentation of the tissue, termed the morphogenetic furrow (MF). The MF passes from the posterior to the anterior of the disc over a period of two days (90 minutes per adjacent row), giving each disc an element of both time and space in development (Fig 1) (Roignant and Treisman 2009). The furrow is initiated by *hedgehog,* which both represses (short range) and activates (long range) *hairy* (Fig 1) (Felsenfeld and Kennison 1995; Strutt and Mlodzik 1997). *hairy* represses *atonal*, preventing precocious neural development anterior to the MF (though this role has

been recently contested) (Brown et al. 1991; Brown, Sattler, Paddock, and Carroll 1995a; Bhattacharya and Baker 2012). *hedgehog* activates the expression of *atonal*, driving the MF anteriorly (Fig 1) (Heberlein et al. 1993; Ma et al. 1993; Struhl 1999). *atonal* is the proneural gene in *Drosophila*, establishing the competency to become photoreceptor cells (Jarman et al. 1994). The relationship between *Delta*/*Notch* and the other members of the pathway is not entirely clear, although in cells posterior to the furrow *Delta/Notch* repress *atonal* (Fig 1) (Firth and Baker 2005; Gavish et al. 2016). There is also some evidence that *Delta*/*Notch* repress negative regulators of *atonal* at the furrow, such as *hairy* (Brown, Sattler, Paddock, and Carroll 1995b; Freeman 2001; Bhattacharya and Baker 2009). In addition, there is some evidence suggesting that *Notch/Delta* are involved in the early stages of *atonal* induction, and alternatively that *atona*l activates its own transcription (Baker and Yu 1997; Dominguez and Hafen 1997; Dominguez et al. 1998; others 1998; Sun et al. 1998; Li and Baker 2001). There are many other genes involved in the specification of the eye disc that will not be mentioned here, in favor of focusing on the genes we have assayed. We analyze the spatial quantitative expression of *hedgehog*, *hairy*, *atonal*, and *Delta* to understand the evolving regulatory logic of the gene network and changes in spatial dynamics between sexes and species.

Variation in gene expression within a species that has no phenotypic effect is termed cryptic variation, and is thought to be a potential source of adaptive mutations when exposed to selection by changing environmental factors (Dworkin et al. 2003; Gibson and Dworkin 2004; Gibson and Reed 2008; Duveau and Felix 2012; Kienle and Sommer 2013; Paaby and Rockman 2014; Lavagnino and Fanara 2015; Taylor and Ehrenreich 2015a). Cryptic variation accumulates due to the robustness of developmental systems to mutational perturbation (Duveau and Felix 2012; Felix 2012; Felix and Barkoulas 2012; Kienle and Sommer 2013; Paaby and Rockman 2014; Paaby and Gibson 2016). Although the final phenotype is the same, the presence of this cryptic variation effects the response to mutational or environmental perturbation, and thus the evolutionary potential of the phenotype. In the past cryptic variation has been experimentally exposed through the use of synthesized genetic backgrounds with large perturbations that prevent buffering of variation (Braendle et al. 2010; Woodruff et al. 2010; Duveau and Felix 2012; Chandler et al. 2014; Taylor and Ehrenreich 2015b).

While this work provides valuable insights into the importance of cryptic variation, cryptic variation in developmental processes in natural genotypes has not been experimentally observed. Here, we will investigate cryptic genetic variation with genotypes and sexes of *D. melanogaster* and *D. simulans* using the four genes from the eye patterning network described above.

When cryptic genetic variation has fixed between species it has been called developmental systems drift, compensatory evolution, and cryptic evolution, here we will refer to it as cryptic evolution (True and Haag 2001; Landry et al. 2005; Felix 2007). These fixed differences do not necessarily result from the fixation of cryptic variation, it can also be due to selection or compensatory mutation (or both) (McGregor et al. 2001; Landry et al. 2005; Goncalves et al. 2012; Martinez et al. 2014; Szamecz et al. 2014; Thompson et al. 2015; Fear et al. 2016). Most often it is investigated in the form of homologous structures that are patterned by different genes, or homologous regulatory regions that have evolved in the composition and placement of binding sites. The most well-known case of homologous structures that are patterned by different genes comes from nematodes, where homologous cells form phenotypically identical adult vulva in different species but are regulated by different molecular mechanisms (Braendle et al. 2010; Duveau and Felix 2012; Felix and Barkoulas 2012; Barkoulas et al. 2013). In the latter case of homologous regulatory regions with conserved expression patterns the most well-known case is the *even-skipped stripe 2* enhancer, where the output is conserved between multiple species of *Drosophila* but the composition and placement of binding sites has diverged (Ludwig et al. 1998; Ludwig et al. 2000). Here we will investigate cryptic evolution on a more micro-evolutionary scale than previously (though it is still a comparison among species) as rather than different genes or enhancer composition evolving between species we will examine spatial quantitative expression level and evolution of the quantitative relationship between genes in the eye patterning network.

We interpret cryptic variation and evolution in quantitative spatial patterns of gene expression in light of regulatory relationships among them. We approach a spatial and quantitative analysis of these gene expression patterns in three ways, first by explicitly creating a spatial gene expression profile and comparing between genotypes, sexes, and species. Second, we were interested in examining if

the regulatory relationship between these genes had evolved between species or harbors variation within a species. Lastly, we investigated the possibility that the spatial relationship between these genes relative to the MF had evolved or harbors variation within populations.

Methods

Fly stocks

D. simulans were collected from the Zuma organic orchard in Zuma beach, CA in the spring of 2012 (Signor et al. *in press*). They were inbred by 15 generations of full sib crosses. *D. melanogaster* were collected in Raleigh, North Carolina and inbred for 20 generations (Mackay et al. 2012).

Image acquisition

Staging and dissection of larvae

All flies were reared on a standard medium at 25° C with a 12-h light/12-h dark cycle. 120 hours after hatching, 3rd instar larva were placed in phosphate buffered saline (PBS) and separated by sex. Their guts were carefully removed posteriorly and their body was inverted anteriorly to expose the brains, eye discs and mouth hooks. After fixation and labeling (described below), eye discs were isolated and mounted.

Hybridization Chain Reaction (HCR)

HCR is unique in that it produces gene expression patterns that are both quantitative and spatial (Supplementary Materials). The DNA probes were designed and synthesized by Molecular Instruments (Choi et al. 2014) (Table S1). Four genes were multiplexed in each preparation as orthogonally-designed hairpins allowed the simultaneous amplification of their target sequences (Fig 1, S1). Each target mRNA was detected using five DNA probes to annotate the position and expression levels for each of the four assayed genes (*hairy, atonal, Delta and hedgehog*).

Each probe contained two-initiator sequences (I1 and I2) that bound to a specific amplifier. While other approaches such as FISH can be adapted to detect individual transcripts, HCR has a linear signal that is 20x brighter than FISH, it reduces non-specific background staining, and it can detect 88% of single RNA molecules in a cell with an appropriately low false discovery rate (Ma and

144 Moses 1995; Pan and Rubin 1995). It is also highly repeatable, with different sets of probes targeted
145 to the same gene showing correlations of .93-.99 (S. Fraser, pers. comm.).

146 The protocol for HCR was modified from (Choi et al. 2014) and is described briefly. The full
147 protocol is available in File S2. Inverted 3rd instar larva were fixed in 4% paraformaldehyde diluted with
148 PBS containing .2% Tween 20 (PBST). After fixation, larva were washed with PBST, then increasing
149 concentrations of methanol (30%, 70% and 100%) at 25° C. Larva were stored in 100% methanol at -
150 20° C. Methanol-fixed samples were thawed, washed with ethanol, re-permeabalized in 60% xylene,
151 washed with ethanol, then methanol and rehydrated with PBST. Samples were permeabalized with
152 proteinase K (4 mg/mL), fixed in 4% formaldehyde then washed with PBST at 25° C. Finally, at 45° C,
153 samples were pre-hybridized for 2 hours before the addition of all the probes. The probe-hybridized
154 larva were placed in wash buffer (Molecular Instruments) at 45° C to remove excess probes.
155 Fluorescently labeled hairpins were snap-cooled then added to the samples at 25° C and placed in the
156 dark to amplify the signal. Afterwards, samples were washed in 5X SSCT solution, isolated in PBST,
157 then placed in Prolong Gold anti-fade mounting medium (Molecular Probes).

158 *Microscopy*

159 Three dimensional images of mounted, HCR stained 3rd instar larva eye discs were acquired on a
160 Zeiss LSM 780 laser scanning microscope (Carl Zeiss MicroImaging, Inc., Thornwood, NY, USA) with
161 Objective Plan-Apochromat 63x/1.40 Oil. The gain was adjusted to avoid pixel saturation.

162 **Extraction of gene expression profiles**

163 *Overview*

164 The first steps in the image analysis is bringing each image to the same orientation and segmenting it.
165 Image segmentation produces a mask in which pixels are assigned to objects or background. Here
166 the objects are one or several mRNA molecules. Then the cellular structure of the imaginal disc is
167 approximated using a hexagonal array. Though the real underlying cell structure of the imaginal disc is
168 technically able to be recognized, this was unsatisfactory in our data due to imaging noise. Thus, at
169 the second step using the R package hexbin we constructed a partition of the imaginal disc area into
170 elements that represent pseudo-cells and have a biologically-relevant hexagonal shape (Brennan et

al. 1998). The number of pseudo-cells was selected by visual inspection of the combined image in which the hexagonal structure was overlaid onto the *atonal* channel to verify fit. We are primarily interested in expression profiles around the MF, providing us a convenient landmark to align images from different preparations, thereby assigning coordinates to the pseudo-cells. However, deformations of the eye disc during growth and preparation sometimes distorts the MF. We used splines to correct for any bending or deformation of the MF. Next, using the histograms of cumulative pixel intensities of objects in expression domains and non-expressing areas we estimated the typical intensity of a transcript and typical background signal, respectively. Consequently, the cumulative intensities greater than the background are divided by the intensity attributed to single mRNA molecule to yield counts of mRNA molecules. This normalizes the expression profiles and corrects for differences in microscope gain between images. Finally, the gene expression profiles are estimated for every pseudo-cell.

Morphological reconstruction and contrast mapping segmentation

To detect gene transcripts within the image stacks we applied a version of the MrComas method that was modified for processing 3D images (Kozlov et al. 2017). This approach first enhances contrast within the image and reduces noise. The images were enlarged by a factor of four with the nearest-neighbor algorithm. They were processed by morphological reconstruction using both opening and closing, where closing (opening) is dilation (erosion) that removes extraneous dark (bright) spots and connects bright (dark) objects (Vincent 1993). The contrast mapping operator assigns each pixel the maximum value between the pixel-by-pixel difference of the reconstructed images and their pixel-by-pixel product and produces the rough mask for each channel. An image, *I*, is mapping from a finite rectangular subset *L* onto the discrete plane Z^2 into a discrete set 0, 1, …, N - 1 of gray levels. Let the dilation δ_B and erosion ϵ_B by structural element *B* be defined as:

$$\delta_B(I) = \bigvee_{\gamma\epsilon_B} I(\gamma) = I \oplus B \qquad \epsilon_B(I) = \bigwedge_{\gamma\epsilon_B} I(\gamma) = I \ominus B$$

Where ∨ and ∧ denote infimum and supremum respectively. Then formulae:

$$\delta^1_{I,B}(J) = (J \oplus B) \wedge I \qquad \epsilon^1_{I,B} = (J \ominus B) \vee I$$

denote geodesic dilation $\delta^1_{I,B}$ and erosion $\epsilon^1_{I,B}$. Binary reconstruction extracts those connected components of the mask image which are marked on the marker image, and in grayscale it extracts

the peaks of the masked image marked by the marker image. Using the dilated masks image I as the marker $J: J = \delta_B(I)$ defines closing by reconstruction:

$$\gamma_B(I) = \epsilon^1_{I,B}\epsilon^1_{I,B} \dots \epsilon^1_{I,B}[\delta_B(I)]$$

Opening by reconstructions uses eroded mask I as a marker J:

$$\phi_B(I) = \delta^1_{I,B}\delta^1_{I,B} \dots \delta^1_{I,B}[\epsilon_B(I)]$$

Then the difference between closing and opening by reconstruction has the meaning of the gradient:

$$\nabla_B(I) = \gamma_B(I) - \phi_B(I)$$

To create strong discontinuities at object edges and flatten signal with the objects the contrast mapping operator takes a maximum between the difference and the pixel-by-pixel produce of the reconstructed images and produces a rough mask for each channel:

$$R = \max\{\nabla_B(I), \gamma_B(I) \odot \phi_B(I)\}$$

Subsequently, this mask was subjected to distance transform, which substituted each pixel value with the number of pixels between it and the closest background pixel. This operation creates 'peaks' and 'valleys' of intensity inside foreground objects. To split erroneously merged objects watershed transform was applied, which treats the whole image as a surface and intensity of each pixel as its height and determines the watershed lines along the tops of ridges separating the catchment basins (Meyer 1994). The quality of segmentation is assessed visually by inspection of the object boarders overlaid with the original image. Finally, each mask is returned to its original size and quantitative measures are made of shape and intensity characteristics such as the number of pixels, as well as their mean and standard deviation in the detected object. MrComas is free and open source software available at http://sourceforge.net/p/prostack/wiki/mrcomas.

Approximating the MF

We defined the position of the MF as the middle of overlap between *hairy* and *atonal* expression. The shape of the MF was approximated with a spline using function smooth.spline in R. The degrees of freedom and other parameters were chosen to make the approximation coincide visually with a MF image.

Inferring counts of transcript number

Segmentation of the image provided a table of coordinates and the shape and intensity characteristics of detected transcripts. Here, we applied filtering steps to remove false positives and determine the count of mRNA transcripts. First, we assumed the object we detected as least intense but most frequent corresponds to a single mRNA molecule. Then, we inferred background intensity for objects outside of well-annotated domains of expression of the four genes. Assuming that the majority of true objects contain a single molecule, we compare the distribution of cumulative intensities of particles in expression domains and areas of known non-expression to obtain the typical intensity of a true single molecule and a false positive, respectively. All detected signals that were lower than the typical intensity of a false positive were removed from the dataset. The number of removed objects is typically less then 10%. All other cumulative pixel intensities were divided by the typical intensity of a true single molecule as normalization coefficient to yield an estimate of the number of mRNA transcripts.

Image registration

We applied an affine coordinate transformation to each eye disc to make the corresponding maxima and the width of expression patterns of four genes in different eyes coincide as closely as possible. To do so, we shifted the coordinate system of each eye to its center and also scaled them in the A-P direction. The center of the pattern in A-P direction is the MF.

We mapped the expression patterns to a unified hexagonal structure in order to make comparisons between pseudo-cells from individual imaginal discs. The unified cell structure was constructed using the R package hexbin. Each cell in the unified grid represents an 'average' cell from individual eyes. The size of a hexagon in the unified grid is greater or equal than the cell size in the individual eye. Thus, the number of molecules in each unified cell in the mapped pattern equals the mean over the cells from native pattern that are covered by this unified cell. After such coordinate transformation, the MF region is defined as 20 cells on either side of the MF, to focus the analysis on the area of interest (the MF).

Filtering and quality controls for each eye disc

Some eye imaginal discs were damaged or deformed in the process of dissection or mounting, resulting in regions of erroneous gene expression, such as disruptions to the MF. The expression profile of each disc was examined by eye and these regions were individually trimmed out of the final dataset. At the edges of each eye disc the pattern of the MF was also degraded, so each eye disc was trimmed dorso-ventrally prior to analysis. Outliers were excluded from the dataset, determined as a single member of the five replicates with more than a 3x difference in expression values. This resulted in a final dataset of 55 eye discs.

Modeling sources of expression variation and evolution

Analysis of individual spatial gene expression patterns

We were primarily interested in variation in gene expression profiles across the eye disc, that is using differences in expression averaged across rows along the *x*-axis. While the *y*-axis is of interest, variation in the shape, size, degree of deformation, and occasional damage to the disc made this analysis intractable. We fit curves to each gene expression profile using the mgcv package in R, using a generalized additive model with integrated smoothness estimation. Smoothing terms are represented using penalized regression splines. predict.gam was used to fit the curves to the original range of values and down sample the curves to eight points. MANOVAs were performed using the "Pillai" test for genotype x sex and species x sex.

Modeling framework to understand variation and evolution of the eye patterning gene network

We wanted to understand if cryptic variation existed within the regulatory logic of *hairy*, *atonal*, *Delta*, and *hedgehog*, or if there had been cryptic evolution between species. To understand the regulatory logic between genes we focused on biologically relevant relationships, such as the regulation of *hairy* by *Delta* and *hedgehog*, but excluded such relationships as *hairy* and *atonal*. This was due to the low overlap between *hairy* and *atonal* expression domains, where including cells where only one or another was expressed would artificially create a relationship between expression levels. Both *hairy* and *atonal* are downstream, directly or indirectly, of *Delta* and *hedgehog* thus it was these relationships that were modeled. We limited the analysis to cells where all genes included were expressed in at least ten molecules.

In the previous analysis, we investigated variation in the cryptic spatial quantitative expression pattern of genes in the MF. Here, we will investigate the possibility that genes in the MF have evolved, or harbor variation, for how they affect each other in particular cells. For example, is high *atonal* expression associated with high expression of *hedgehog*, given that *hedgehog* activates *atonal*? We used the following equations to determine the relationship between the expression of these genes:

$$hairy(i,s) = k^{Dl} \times Dl(i,s) + k^{hh} \times hh(i,s) + \alpha$$

$$atonal(i,s) = k^{Dl} \times Dl(i,s) + k^{hh} \times hh(i,s) + \alpha$$

The coefficient k and constant α were fit using standard methods for multiple regression. Here $hairy(i,s)$ and $atonal(i,s)$ are the measured expression level of each gene in cell i in individual s. $Dl(i,s)$ and $hh(i,s)$ are vectors containing the corresponding expression levels of *hairy* and *atonal*'s regulators *Delta* and *hedgehog*. To determine if the regulatory logic is the same between genotypes and species we can then use the regression coefficients from these models in a MANOVA. We note that we cannot exclude the possibility that other unmeasured genes are responsible for producing this variation.

Model for understanding overall variation and evolution of MF structure

Lastly, we wanted to understand if there is cryptic variation and/or evolution for the relationship between the MF and gene expression, or if cryptic variation and/or evolution existed for the size of the MF overall. For example, the MF was called as the position of overlap between *atonal* and *hairy* expression, but it is unclear how the overall gene expression pattern of these genes relates to their overlap. For example, is the position of maximum expression of each always the same relative to the MF? Two processes occurred to make the MF comparable between samples, they were shifted to occupy the same position depending upon the position of overlap of *hairy* and *atonal*, and they were scaled to occupy the same total area. The amount required to scale will depend both on the size of the original disc and the width of the MF relative to the disc. To account for differences in size we include

the number of rows in the original disc prior to any transformations as a cofactor and perform ANOVA in R.

RESULTS

Individual spatial gene expression patterns

First, to characterize the spatiotemporal dynamics of transcriptional activity along the anterior-posterior axis, we took the spatial average of signal across the dorsal-ventral axis and compared between genotypes, sexes, and species (Fig 2A). We found abundant cryptic spatial quantitative variation in expression profiles (Fig 2-3). The expression profile of *hairy* around the MF harbors cryptic variation between genotypes and there is an interaction between genotype and sex (Table 1, $p = 2 \times 10^{-3}$, $p = 0.02$). There has also been cryptic evolution between species for *hairy* (Table 1, $p = 3 \times 10^{-4}$). While *atonal* has not evolved between species, there is cryptic variation in expression profile between genotypes, sexes, and there is an interaction between genotype and sex (Fig 3A-C, Table 1, $p = 4 \times 10^{-4}$, $p = .02$, $p = .02$). Surprisingly, given the conservation of *Delta* in general, *Delta* harbors variation in spatial quantitative expression behind the MF between genotypes and sexes (Table 1, $p = 2 \times 10^{-3}$, $p = 7 \times 10^{-4}$) and there are significant interactions between genotype and sex (Fig 2B-C, Table 1, $p = 2 \times 10^{-3}$). There has also been cryptic evolution of *Delta* between species, and evolution of the interaction between species and sex (Table 1, $p = .03$, $p = 3 \times 10^{-4}$). *hedgehog* is not different between species but is significantly different between genotypes, sexes, and there is an interaction between the two (Table 1, $p = 5 \times 10^{-4}$, $p = .05$, $p = 1 \times 10^{-3}$). There is also a significant interaction between species and sex (Table 1, $p = .01$).

Thus, *hairy* and *Delta* have cryptically evolved different spatial quantitative expression patterns between species, while *hairy*, *atonal*, *Delta*, and *hedgehog* harbor cryptic variation within species and sexes. Given that there are regulatory relationships between these genes, it is interesting to see that they do not all harbor variation for the same factors. This could potentially be due to the influence of other unmeasured regulatory factors, or to variation in the relationship between these genes and other components in the gene regulatory network.

Variation and evolution of the eye patterning gene network

There has been cryptic evolution in the regulatory logic of *hairy* and its upstream regulators *Delta* and *hedgehog* between species (Fig 4A-C, Table 2, p = .03). There is also cryptic variation between sexes in the regulatory logic of *hairy* and its upstream regulators *Delta* and *hedgehog* (Table 2, p = .03). There has been significant evolution of the regulatory logic of *atonal*, in a significant interaction between species and sex ($p = 1 \times 10^{-3}$). Furthermore, while there was no significant effect of genotype for *hairy*, there is for *atonal*, indicating that there is cryptic variation segregating in the population effecting the relationship between *atonal, hedgehog*, and *Delta* ($p = 1.6 \times 10^{-5}$). There is also a significant interaction between genotype and sex ($p = 1 \times 10^{-3}$). Thus, the relationship between *hairy* and *atonal* and their regulators has cryptically evolved between species and sexes in *hairy*, and between genotypes and sex in *atonal* (cryptic variation). We illustrate this difference between species in Figure 3, where a different relationship between *hairy* and *hedgehog* is visible between *D. melanogaster* and *D. simulans*. In brief, the frequency of cells with a given log transformed level of expression are plotted against one another for *hairy* and *hedgehog*. *hairy* is primarily expressed anterior to the MF and *hedgehog* posterior, and they have a different regulatory relationship in each region with *hedgehog* activating *hairy* long range (anterior) and repressing it short range (posterior). This is reflected in the frequency of cells expressing both genes for *D. melanogaster*, where anterior to the MF there is a high frequency of *hairy* expressing cells and a low frequency of co-occurring high *hedgehog* expression. Posterior to the MF the opposite is true, with high expression of *hedgehog* lacking concordance with any expression of *hairy*. In *D. simulans*, posterior to the MF, this relationship is the same as in *D. melanogaster*. However, in anterior to the MF this is not the case. Expression of *hairy* and *hedgehog* both increase as the other increases, with widespread co-occurrence.

Variation and evolution of MF structure

The amount that they were shifted is not significant for genotype, sex, or species, suggesting that the relationship of maximum gene expression with the MF does not vary. However, the amount that they were scaled is, after accounting for original differences in size, between species ($p = 1.38 \times 10^{-6}$).

359 This suggests that the total relative width of the MF varies between species, but not between
360 genotypes or sexes. This is also suggestive of evolving interrelationships among genes that could
361 result in broader or narrower areas in which they enhance or suppress expression of one another.

362 **Discussion**

363 Our results summarize a complicated pattern of variation sorting in the gene network involved in
364 patterning the MF. For example, the overall shape of the expression of *hedgehog* across the eye disc
365 is different between genotypes, sexes, and there is an interaction between species and sex and
366 genotype and sex. *hedgehog* upregulates *hairy*, but *hairy* has differences in expression between
367 species (which *hedgehog* does not), genotypes, and there is an interaction between genotype and
368 sex. Thus, there is no propagation of the pattern seen in *hedgehog* through the network. In another
369 example, *Delta/Notch* is expected to repress *atonal*, but while *Delta/Notch* is significant for all
370 categories tested *atonal* is only significant for genotype, sex, and their interaction. It is possible that
371 this variation is being mitigated or dampened by other regulatory factors not assayed here, or that
372 certain aspects of genetic background are more or less sensitive to variation. For example, that fixed
373 variation between species dampens variation at *Delta/Notch* but sorting variation remains sensitive
374 between genotypes, which propagates to *atonal*.

375 It may be that all of this variation is within levels tolerated by the network, as it has been shown
376 that gene networks can have thresholds of variation, below which differences in expression are
377 effectively neutral. These thresholds can also be two sided, creating a sigmoidal curve the center of
378 which is neutral phenotypic space (Felix and Barkoulas 2015). Many studies have shown a relative
379 insensitivity to variation in gene dosage, for example in *Drosophila* early embryos the *bicoid* gradient
380 results in normal development at one to four dosages of the gene, but markedly abnormal
381 development at six or more (Namba et al. 1997; Liu et al. 2013; Lucas et al. 2013). It is also possible
382 that the cryptic evolution documented in these genes is in fact deleterious, and is being compensated
383 for elsewhere in the network. While most deleterious mutations are purged by selection, they may rise
384 in frequency due to genetic drift or hitchhiking, among other possible causes (McKenzie and Clarke
385 1988; Burch and Chao 1999; Estes and Lynch 2003; Chun and Fay 2011). This type of compensatory

386 mutation has been documented in microbial and animal systems (McKenzie et al. 1982; McKenzie
387 1993; Burch and Chao 1999; Moore et al. 2000; Estes and Lynch 2003; Maisnier-Patin and Andersson
388 2004; Stoebel et al. 2009; Brown et al. 2010; Charusanti et al. 2010; Estes et al. 2011; Szamecz et al.
389 2014). Recently cell cycle heterogeneity has been implicated in the appearance of widespread noise
390 in development, though that is less of problem here given that cell division is synchronized posterior
391 the MF and cells are at GI arrest within the MF (Kumar 2013; Keren et al. 2015).

392 Other than differences in the allometric relationship of eyes between males and females there has
393 been no documentation of sexual dimorphism in *Drosophila* eyes, which could potentially contribute to
394 the differences between sexes seen for some of the genes in the MF. However, we note that we
395 controlled for size of the imaginal disc in this study and the difference between males and females
396 seems to largely be driven by differences in maximum expression. Furthermore, the size of the eye
397 disc was not consistently significantly different between sexes. By one account female eyes in *D.*
398 *melanogaster* are smaller than expected based on allometry, while other work finds that the opposite
399 is the case in both *D. melanogaster* and *D. simulans* (Cowley and Atchley 1988; Posnien et al. 2012).
400 Body size is at least in part controlled by *Sex-lethal,* and sex specific development in somatic tissues
401 are governed by *doublesex* (Rideout et al. 2010; Mathews et al. 2017). We have detected *doublesex*
402 expression in the eye anterior to the MF, in cells prior to cell cycle arrest at the MF (Fig S2). It is
403 possible that an interaction between *doublesex* and *hairy*, *atonal*, *Delta*, or *hedgehog* is mediating the
404 change in cryptic evolution in regulatory logic between sexes. It is also possible that some of this
405 variation is not cryptic, and in fact has an undocumented effect on sex-specific development of the
406 eyes.

407 There have been other semi-quantitative approaches to studying spatial gene expression
408 patterns. In another study on *orthodenticle*, the authors found that the spatial and temporal pattern of
409 gene expression was conserved but the amount of gene product was not, though this work was not
410 strictly quantitative given that measurements were from *in situ* hybridization and reporter constructs
411 (Palsson et al. 2014). This is in contrast to our results which showed significant differences in the
412 spatial relationship between gene expression patterns between species. Other semi-quantitative

works on the *Drosophila* embryo using *in situ* hybridization found that the regulatory relationship between genes in the anterior-posterior blastoderm patterning network were conserved, despite differences between species in their spatio-temporal pattern (Fowlkes et al. 2011; Wunderlich et al. 2012). Here we find that the regulatory relationship between *atonal* and *hairy*, and their regulators *hedgehog* and *Delta*, has evolved between species, sexes, and genotypes.

In the past, the developmental approach to understanding gene networks has been to analyze large effect mutations and their qualitative downstream effects. This results in robust data on perturbed regulatory networks, but obfuscates information on more normal interrelationships among genes. Similarly, the evolutionary approach to development generally targets large changes that have occurred over broad phylogenetic distances (Kopp et al. 2000; Jeong et al. 2008; Rosenblum et al. 2010; Reed et al. 2011; Ito et al. 2013; Signor, Li, et al.; Yassin et al.). Here we take an entirely different approach by focusing on small, quantitative variation between genotypes and closely related species (Johnson 2006; Nunes et al. 2013). Using this approach, we were able to quantify the regulatory relationships among genes and to observe how these relationships are altered between genotypes, sexes and species. Reconciling the speed of this cryptic developmental evolution with the patterns of molecular evolution in the underlying genes will yield new insights on the rules governing microevolution of gene regulatory networks.

AUTHOR CONTRIBUTIONS: S. A. performed the staining and imaging of the eye discs, K. K. processed the imaging data, S.S. conceived of the experiment, analyzed the processed data and wrote the paper, S. N. conceived of the experiment, coordinated the research, and co-wrote the paper.

ACKNOWLEDGEMENTS: The authors thank S. Restrepo, M. Samsonova, P. Marjoram, J. Butler, G. Mackerel, R. Hudson, and E. Williams for help with experimental procedures and manuscript preparation. This work was supported by grants U01GM103804 and RO1GM102227 to S.V.

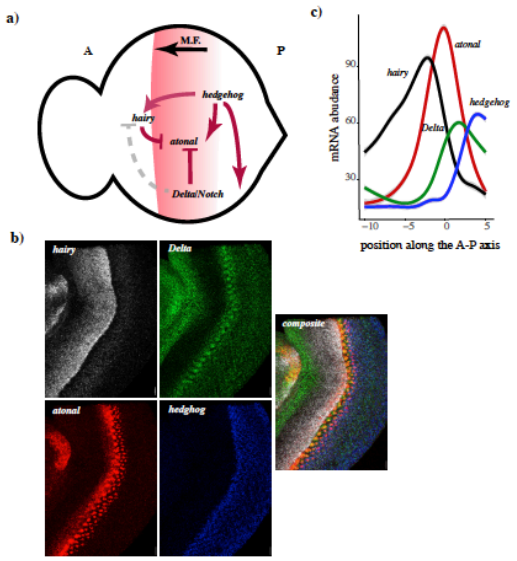

Figure 1. **a)** A summary of the eye patterning genes and pathway explored in this paper. The position of the MF is shown in red, and its direction of movement indicated below. Regulatory relationships are illustrated either as repression (bar) or activation (arrow). Regulatory relationships which are unclear are shown as gray dotted lines. **b)** Example images from the dataset, illustrating gene expression patterns of each gene. The composite image makes the additional point that we were able to analyze co-expression patterns of all four genes without needing to stain each gene in different samples and infer gene co-expression patterns. **c)** An illustration of the general expression pattern of each of the four genes in the study, along the anterior-posterior axis of the eye disc.

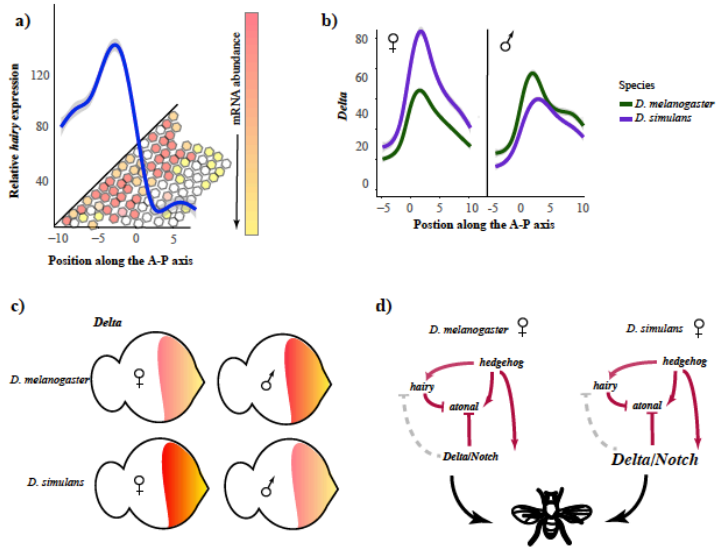

Figure 2. **a)** This is an example of a curve being fitted to the gene expression profiles, though note that the curve corresponds to the average in a given row (*x*-axis). The hexagons are intended to represent cells with varying amounts of *hairy* expression, from the highest (red) to the lowest (white). **b)** An illustration of variation in *Delta* expression between species and sexes. Curves shown are fitted to all genotypes within a sex and species with confidence intervals indicated in gray. **c)** An illustration using the imaginal disc of how *Delta* expression varied between species and sexes, with lower expression in *D. melanogaster* females and *D. simulans* males **d)** Cryptic evolution of *Delta* illustrated within the context of the gene network, illustrating how changes in *Delta* expression are not perturbing the gene network and result in phenotypically normal *Drosophila*.

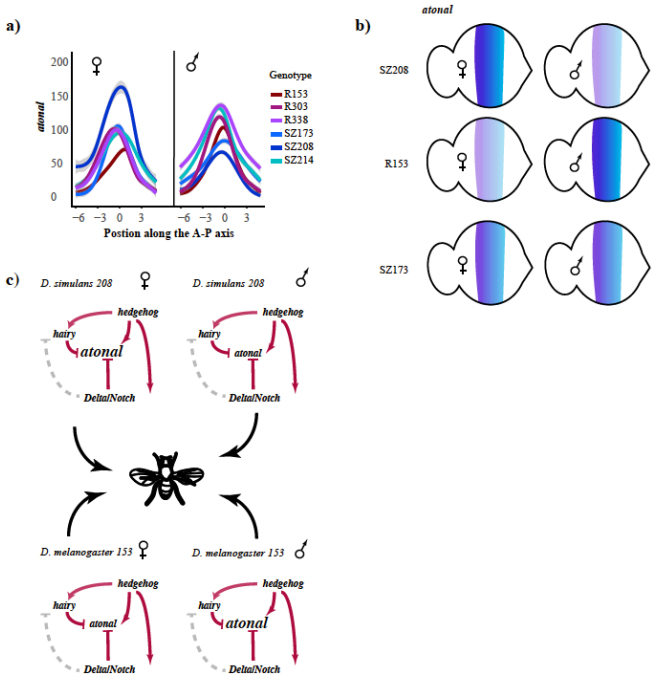

Figure 3. **a)** An illustration of cryptic variation in *atonal* expression between genotypes and sexes. Curves shown are fitted to each genotype and sex with confidence intervals indicated in gray. **c)** An illustration using the imaginal disc of how *atonal* expression varied between genotypes, with lower expression in females of *D. melanogaster* R153 and males of *D. simulans* Sz208. *D. simulans* Sz173 has lower expression than females of Sz208 but it is not sexually dimorphic. **d)** Cryptic evolution of *atonal* illustrated within the context of the gene network, illustrating how changes in *atonal* expression are not perturbing the gene network and result in phenotypically normal *Drosophila*.

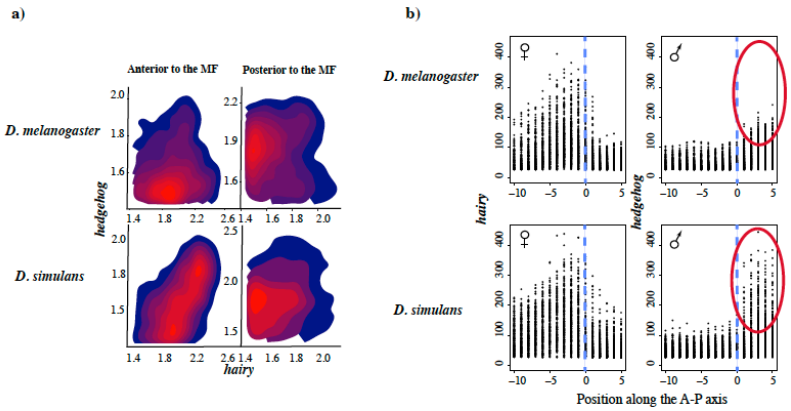

Figure 4. **a)** An example of cryptic variation in regulatory logic between *D. simulans* and *D. melanogaster* for *hairy* and *hedgehog*. The heat map illustrates the density of points, and thus reflects the frequency of a given co-expression profile between *hairy* and *hedgehog*. Gene expression values were log-transformed to better illustrate lower values and split between anterior to the MF and posterior to the MF. The split between the two regions was to investigate the possibility that *hedgehog* had a different regulatory relationship with *hairy* depending upon its relationship to the MF, given that *hedgehog* is thought to activate *hairy* long range and repress *hairy* short range. **b)** An illustration of the change in quantitative spatial expression of *hairy* and *hedgehog* between species and sexes, with the position of the center of the MF marked with a dotted blue line. The red circle emphasizes a large change in maximum *hedgehog* expression in males of the two species.

hairy

Effect	*numDF*	*denDF*	F-value	*p*-value
Species	8	35	5.1	**3×10^{-4}**
Genotype	32	152	2.07	**2×10^{-3}**
Sex	8	35	1.08	0.32
Species x Sex	8	35	1.94	0.08
Genotype x Sex	32	152	1.73	**0.02**

atonal

Effect	*numDF*	*denDF*	F-value	*p*-value
Species	8	35	1.53	0.18
Genotype	32	152	2.31	**4×10^{-4}**
Sex	8	35	2.6	0.02
Species x Sex	8	35	1.91	0.09
Genotype x Sex	32	152	1.73	**0.02**

Delta

Effect	*numDF*	*denDF*	F-value	*p*-value
Species	8	35	2.43	**0.03**
Genotype	32	152	2.07	**2×10^{-3}**
Sex	8	35	4.55	**7×10^{-4}**
Species x Sex	8	35	5.03	**3×10^{-4}**
Genotype x Sex	32	152	2.03	**2×10^{-3}**

hedgehog

Effect	*numDF*	*denDF*	F-value	*p*-value
Species	8	35	0.87	0.55
Genotype	32	152	2.28	**5×10^{-4}**
Sex	8	35	2.23	0.05
Species x Sex	8	35	2.88	0.01
Genotype x Sex	32	152	2.17	**1×10^{-3}**

Table 1: The results of the full model for each gene, significant *p*-values are indicated in bold, with gray shading.

hairy

Effect	*numDF*	*denDF*	F-value	*p*-value
Species	2	41	4.03	**0.25**
Genotype	8	84	1.2	0.31
Sex	2	41	3.95	**0.027**
Species x Sex	2	41	0.78	0.46
Genotype x Sex	8	84	1,11	0.37

atonal

Effect	*numDF*	*denDF*	F-value	*p*-value
Species	2	41	2.64	0.08
Genotype	8	84	5.43	**1.6×10^{-5}**
Sex	2	41	0.67	0.52
Species x Sex	2	41	8.09	**1×10^{-3}**
Genotype x Sex	8	84	2.41	**0.02**

Table 2: The results of the full model investigating changes in the regulatory relationship between *hairy*, *Delta*, and *hedgehog*, and *atonal*, *Delta*, and *hedgehog*. Significant *p*-values are indicated in bold, with gray shading.

488

Atkins M, Jiang Y, Sansores-Garcia L, Jusiak B, Halder G, Mardon G. 2013. Dynamic Rewiring of the Drosophila Retinal Determination Network Switches Its Function from Selector to Differentiation.Desplan C, editor. PLoS Genet. 9:e1003731–17.

Baker NE, Yu SY. 1997. Proneural function of neurogenic genes in the developing Drosophila eye. Curr. Biol. 7:122–132.

Barkoulas M, van Zon JS, Milloz J, van Oudenaarden A, Felix M-A. 2013. Robustness and Epistasis in the C. elegans Vulval Signaling Network Revealed by Pathway Dosage Modulation. Dev. Cell 24:64–75.

Bhattacharya A, Baker NE. 2009. The HLH protein Extramacrochaetae is required for R7 cell and cone cell fates in the Drosophila eye. Dev. biol. 327:288–300.

Bhattacharya A, Baker NE. 2012. The Role of the bHLH Protein Hairy in Morphogenetic Furrow Progression in the Developing Drosophila Eye.Hassan BA, editor. PLoS ONE 7:e47503–e47505.

Braendle C, Baer CF, Felix M-A. 2010. Bias and evolution of the mutationally accessible phenotypic space in a developmental system.Barsh GS, editor. PLoS Genet. 6:e1000877–13.

Brennan CA, Ashburner M, Moses K. 1998. Ecdysone pathway is required for furrow progression in the developing Drosophila eye. Development 125:2653–2664.

Brown KM, Costanzo MS, Xu W, Roy S, Lozovsky ER, Hartl DL. 2010. Compensatory Mutations Restore Fitness during the Evolution of Dihydrofolate Reductase. Mol. Biol. Evol. 27:2682–2690.

Brown NL, Sattler CA, Markey DR, Carroll SB. 1991. hairy gene function in the Drosophila eye: normal expression is dispensable but ectopic expression alters cell fates. Development 113:1245–1256.

Brown NL, Sattler CA, Paddock SW, Carroll SB. 1995a. Hairy and emc negatively regulate morphogenetic furrow progression in the Drosophila eye. Cell 80:879–887.

Brown NL, Sattler CA, Paddock SW, Carroll SB. 1995b. Hairy and emc negatively regulate morphogenetic furrow progression in the Drosophila eye. Cell 80:879–887.

Burch CL, Chao L. 1999. Evolution by small steps and rugged landscapes in the RNA virus phi6. Genetics 151:921–927.

Chandler CH, Chari S, Tack D, Dworkin I. 2014. Causes and consequences of genetic background effects illuminated by integrative genomic analysis. Genetics 196:1321–1336.

Charusanti P, Conrad TM, Knight EM, Venkataraman K, Fong NL, Xie B, Gao Y, Palsson BØ. 2010. Genetic Basis of Growth Adaptation of Escherichia coli after Deletion of pgi, a Major Metabolic Gene.Casadesús J, editor. PLoS Genet. 6:e1001186–13.

Choi HMT, Beck VA, Pierce NA. 2014. Next-generation in situ hybridization chain reaction: higher gain, lower cost, greater durability. ACS Nano 8:4284–4294.

Chun S, Fay JC. 2011. Evidence for hitchhiking of deleterious mutations within the human genome.Pritchard JK, editor. PLoS Genet. 7:e1002240.

Cowley DE, Atchley WR. 1988. Quantitative Genetics of Drosophila Melanogaster. II. Heritabilities and Genetic Correlations between Sexes for Head and Thorax Traits. Genetics 119:421–433.

526 Dominguez M, Hafen E. 1997. Hedgehog directly controls initiation and propagation of retinal
527 differentiation in the Drosophila eye. Genes Dev. 11:3254–3264.

528 Dominguez M, Wasserman JD, Freeman M. 1998. Multiple functions of the EGF receptor in
529 Drosophila eye development. Curr. Biol. 8:1039–1048.

530 Duveau F, Felix M-A. 2012. Role of Pleiotropy in the Evolution of a Cryptic Developmental Variation in
531 Caenorhabditis elegans.Noor MAF, editor. PLoS Biol. 10:e1001230–19.

532 Dworkin I, Palsson A, Birdsall K, Gibson G. 2003. Evidence that Egfr Contributes to Cryptic Genetic
533 Variation for Photoreceptor Determination in Natural Populations of Drosophila melanogaster.
534 Curr. Biol. 13:1888–1893.

535 Estes S, Lynch M. 2003. Rapid fitness recovery in mutationally degraded lines of Caenorhabditis
536 elegans. Evolution 57:1022–1030.

537 Estes S, Phillips PC, Denver DR. 2011. Fitness recovery and compensatory evolution in natural
538 mutant lines of C. elegans. Evolution 65:2335–2344.

539 Fear JM, León-Novelo LG, Morse AM, Gerken AR, Van Lehmann K, Tower J, Nuzhdin SV, McIntyre
540 LM. 2016. Buffering of Genetic Regulatory Networks in Drosophila melanogaster. Genetics
541 203:1177–1190.

542 Felix M-A, Barkoulas M. 2012. Robustness and flexibility in nematode vulva development. Trends
543 Genet. 28:185–195.

544 Felix M-A, Barkoulas M. 2015. Pervasive robustness in biological systems. Nat. Rev. Genet. 16:483–
545 496.

546 Felix M-A. 2007. Cryptic Quantitative Evolution of the Vulva Intercellular Signaling Network in
547 Caenorhabditis. Curr. Biol. 17:103–114.

548 Felix M-A. 2012. Evolution in developmental phenotype space. Current Opinion in Genetics &
549 Development 22:593–599.

550 Felsenfeld AL, Kennison JA. 1995. Positional signaling by hedgehog in Drosophila imaginal disc
551 development. Development 121:1–10.

552 Firth LC, Baker NE. 2005. Extracellular Signals Responsible for Spatially Regulated Proliferation in the
553 Differentiating Drosophila Eye. Dev. Cell 8:541–551.

554 Fowlkes CC, Eckenrode KB, Bragdon MD, Meyer M, Wunderlich Z, Simirenko L, Luengo Hendriks CL,
555 Keranen SVE, Henriquez C, Knowles DW, et al. 2011. A Conserved Developmental Patterning
556 Network Produces Quantitatively Different Output in Multiple Species of Drosophila.Kopp A,
557 editor. PLoS Genet. 7:e1002346.

558 Freeman ABAM. 2001. Notch signalling and the initiation of neural development in the Drosophila
559 eye. :1–10.

560 Gavish A, Shwartz A, Weizman A, Schejter E, Shilo B-Z, Barkai N. 2016. Periodic patterning of the
561 Drosophila eye is stabilized by the diffusible activator Scabrous. Nat. Comm. 7:1–10.

562 Gibson G, Dworkin I. 2004. Uncovering cryptic genetic variation. Nat. Rev. Genet. 5:681–690.

563 Gibson G, Reed LK. 2008. Cryptic genetic variation. Curr. Biol. 18:R989–R990.

564 Gibson G. 2009. Decanalization and the origin of complex disease. Nat. Rev. Genet. 10:134–140.

565 Goncalves A, Leigh-Brown S, Thybert D, Stefflova K, Turro E, Flicek P, Brazma A, Odom DT, Marioni
566 JC. 2012. Extensive compensatory cis-trans regulation in the evolution of mouse gene expression.
567 Genome Res. 22:2376–2384.

568 Heberlein U, Wolff T, Rubin GM. 1993. The TGF[beta] homolog dpp and the segment polarity gene
569 hedgehog are required for propagation of a morphogenetic wave in the Drosophila retina. 75:913–
570 926.

571 Hu JX, Thomas CE, Brunak S. 2016. Network biology concepts in complex disease comorbidities.
572 Nat. Rev. Genet. 17:615–629.

573 Ito Y, Harigai A, Nakata M, Hosoya T, Araya K, Oba Y, Ito A, Ohde T, Yaginuma T, Niimi T. 2013. The
574 role of doublesex in the evolution of exaggerated horns in the Japanese rhinoceros beetle. Nat.
575 Neurosci. 14:561–567.

576 Jarman AP, Grell EH, Ackerman L, Jan LY, Jan YN. 1994. atonal is the proneural gene for Drosophila
577 photoreceptors. Nature 369:398–400.

578 Jeong S, Rebeiz M, Andolfatto P, Werner T, True J, Carroll SB. 2008. The evolution of gene
579 regulation underlies a morphological difference between two *Drosophila* sister species. Cell
580 132:783–793.

581 Johnson NA. 2006. The Micro-evolution of development. Genetica 129:1–5.

582 Keren L, van Dijk D, Weingarten-Gabbay S, Davidi D, Jona G, Weinberger A, Milo R, Segal E. 2015.
583 Noise in gene expression is coupled to growth rate. Genome Res. 25:1893–1902.

584 Kienle S, Sommer RJ. 2013. Cryptic variation in vulva development by cis-regulatory evolution of a
585 HAIRY-binding site. Nat. Comm. 4:1714.

586 Kopp A, Duncan I, Godt D, Carroll SB. 2000. Genetic control and evolution of sexually dimorphic
587 characters in *Drosophila*. Nature 408:553–559.

588 Kozlov K, Kosheverova V, Kamentseva R, Kharchenko M, Sokolkova A, Kornilova E, Samsonova M.
589 2017. Quantitative analysis of the heterogeneous population of endocytic vesicles. J. Bioinform.
590 Comput. Biol. 10:1750008.

591 Kumar JP. 2013. Catching the Next Wave: Patterning of the Drosophila Eye by the Morphogenetic
592 Furrow. In: Molecular Genetics of Axial Patterning, Growth and Disease in the Drosophila Eye.
593 New York, NY: Springer New York. pp. 75–97.

594 Landry CR, Wittkopp PJ, Taubes CH, Ranz JM, Clark AG, Hartl DL. 2005. Compensatory *cis-trans*
595 evolution and the dysregulation of gene expression in interspecific hybrids of *Drosophila*. Genetics
596 171:1813–1822.

597 Lavagnino NJ, Fanara JJ. 2015. Changes Across Development Influence Visible and Cryptic Natural
598 Variation of Drosophila melanogaster Olfactory Response. Evolutionary biology 43:96–108.

599 Li W, Ohlmeyer JT, Lane ME, Kalderon D. 1995. Function of protein kinase A in hedgehog signal
600 transduction and Drosophila imaginal disc development. Cell 80:553–562.

601 Li Y, Baker NE. 2001. Proneural enhancement by Notch overcomes Suppressor-of-Hairless repressor
602 function in the developing Drosophila eye. Curr. Biol. 11:330–338.

603 Liu F, Morrison AH, Gregor T. 2013. Dynamic interpretation of maternal inputs by the Drosophila
604 segmentation gene network. Proc. Nat. Acad. Sci. USA 110:6724–6729.

605 Lucas T, Ferraro T, Roelens B, Las Heras Chanes De J, Walczak AM, Coppey M, Dostatni N. 2013.
606 Live Imaging of Bicoid-Dependent Transcription in Drosophila Embryos. Curr. Biol. 23:2135–2139.

607 Ludwig MZ, Bergman C, Patel NH, Kreitman M. 2000. Evidence for stabilizing selection in a eukaryotic
608 enhancer element. Nature 403:564–567.

609 Ludwig MZ, Patel NH, Kreitman M. 1998. Functional analysis of eve stripe 2 enhancer evolution in
610 Drosophila: rules governing conservation and change. Development 125:949–958.

611 Ma C, Moses K. 1995. Wingless and patched are negative regulators of the morphogenetic furrow and
612 can affect tissue polarity in the developing Drosophila compound eye. Development 121:2279–
613 2289.

614 Ma C, Zhou Y, Beachy PA, Moses K. 1993. The segment polarity gene hedgehog is required for
615 progression of the morphogenetic furrow in the developing Drosophila eye. Cell 75:927–938.

616 Mackay TFC, Richards S, Stone EA, Barbadilla A, Ayroles JF, Zhu D, Casillas S, Han Y, Magwire
617 MM, Cridland JM, et al. 2012. The Drosophila melanogaster Genetic Reference Panel. Nature
618 482:173–178.

619 Maisnier-Patin S, Andersson DI. 2004. Adaptation to the deleterious effects of antimicrobial drug
620 resistance mutations by compensatory evolution. Research in Microbiology 155:360–369.

621 Martinez C, Rest JS, Kim A-R, Ludwig M, Kreitman M, White K, Reinitz J. 2014. Ancestral
622 Resurrection of the Drosophila S2E Enhancer Reveals Accessible Evolutionary Paths through
623 Compensatory Change. Mol. Biol. Evol. 31:903–916.

624 Mathews KW, Cavegn M, Zwicky M. 2017. Sexual dimorphism of body size is controlled by dosage of
625 the X-chromosomal gene Myc and by the sex-determining gene tra in Drosophila. Genetics.

626 McGregor AP, Shaw PJ, Hancock JM, Bopp D, Hediger M, Wratten NS, Dover GA. 2001. Rapid
627 restructuring of bicoid-dependent hunchback promoters within and between Dipteran species:
628 implications for molecular coevolution. Evolution \& Development 3:397–407.

629 McKenzie JA, Clarke GM. 1988. Diazinon resistance, fluctuating asymmetry and fitness in the
630 Australian sheep blowfly, lucilia cuprina. Genetics 120:213–220.

631 McKenzie JA, Whitten MJ, Adena MA. 1982. The effect of genetic background on the fitness of
632 diazinon resistance genotypes of the Australian sheep blowfly, Lucilia cuprina. Heredity 49:1–9.

633 McKenzie JA. 1993. Measuring fitness and intergenic interactions: The evolution of resistance to
634 diazinon inLucilia cuprina. Genetica 90:227–237.

635 Meyer F. 1994. Topographic distance and watershed lines. Signal processing 38:113–125.

636 Moore FB, Rozen DE, Lenski RE. 2000. Pervasive compensatory adaptation in Escherichia coli. Proc.
637 R. Soc. B 267:515–522.

638 Namba R, Pazdera TM, Cerrone RL, Minden JS. 1997. Drosophila embryonic pattern repair: how
639 embryos respond to bicoid dosage alteration. Development 124:1393–1403.

640 Nunes MDS, Arif S, Schlötterer C, McGregor AP. 2013. A perspective on micro-evo-devo: progress
641 and potential. Genetics 195:625–634.

642 others SSA. 1998. Regulation of EGF receptor signaling establishes pattern across the developing
643 Drosophila retina. :1–14.

644 Paaby A, Gibson G. 2016. Cryptic Genetic Variation in Evolutionary Developmental Genetics. Biology
645 5:28–13.

646 Paaby AB, Rockman MV. 2014. Cryptic genetic variation: evolution's hidden substrate. Nat. Rev.
647 Genet. 15:247–258.

648 Palsson A, Wesolowska N, Reynisdóttir S, Ludwig MZ, Kreitman M. 2014. Naturally Occurring
649 Deletions of Hunchback Binding Sites in the Even-Skipped Stripe 3+7 Enhancer.Moses AM,
650 editor. PLoS ONE 9:e91924–15.

651 Pan D, Rubin GM. 1995. cAMP-dependent protein kinase and hedgehog act antagonistically in
652 regulating decapentaplegic transcription in Drosophila imaginal discs. Cell 80:543–552.

653 Posnien N, Hopfen C, Hilbrant M, Ramos-Womack M, Murat S, Schönauer A, Herbert SL, Nunes
654 MDS, Arif S, Breuker CJ, et al. 2012. Evolution of Eye Morphology and Rhodopsin Expression in
655 the Drosophila melanogaster Species Subgroup.Flatt T, editor. PLoS ONE 7:e37346–11.

656 Raj A, van den Bogaard P, Rifkin SA, van Oudenaarden A, Tyagi S. 2008. Imaging individual mRNA
657 molecules using multiple singly labeled probes. Nat. Meth. 5:877–879.

658 Reed RD, Papa R, Martin A, Hines HM, Counterman BA, Pardo-Diaz C, Jiggins CD, Chamberlain NL,
659 Kronforst MR, Chen R, et al. 2011. optix Drives the Repeated Convergent Evolution of Butterfly
660 Wing Pattern Mimicry. Science 333:1137–1141.

661 Rideout EJ, Dornan AJ, Neville MC, Eadie S, Goodwin SF. 2010. Control of sexual differentiation and
662 behavior by the *doublesex* gene in *Drosophila* melanogaster. Nat. Neurosci. 13:458–466.

663 Roignant J-Y, Treisman JE. 2009. Pattern formation in the Drosophila eye disc. Int. J. Dev. Biol.
664 53:795–804.

665 Rosenblum EB, Römpler H, Schöneberg T, Hoekstra HE. 2010. Molecular and functional basis of
666 phenotypic convergence in white lizards at White Sands. Proc. Nat. Acad. Sci. USA 107:2113–
667 2117.

668 Shah S, Lubeck E, Schwarzkopf M, He TF. 2016. Single-molecule RNA detection at depth via
669 hybridization chain reaction and tissue hydrogel embedding and clearing. Genetics.

670 Signor SA, Li Y, Rebeiz M, Kopp A. Genetic convergence in the evolution of male-specific color
671 patterns in Drosophila

672 . Curr. Biol.

673 Signor SA, New F, Nuzhdin S. An abundance of high frequency variance uncovered in a large panel
674 of Drosophila simulans. Heredity.

675 Stoebel DM, Hokamp K, Last MS, Dorman CJ. 2009. Compensatory Evolution of Gene Regulation in
676 Response to Stress by Escherichia coli Lacking RpoS.Guttman DS, editor. PLoS Genet.
677 5:e1000671–e1000679.

678 Struhl SGAG. 1999. Progression of the morphogenetic furrow in the Drosophila eye: the roles of
679 Hedgehog, Decapentaplegic and the Raf pathway. :1–14.

680 Strutt DI, Mlodzik M. 1997. Hedgehog is an indirect regulator of morphogenetic furrow progression in
681 the Drosophila eye disc. Development 124:3233–3240.

682 Sun Y, Jan LY, Jan YN. 1998. Transcriptional regulation of atonal during development of the
683 Drosophila peripheral nervous system. Development 125:3731–3740.

684 Szamecz B, Boross G, Kalapis D, Kovács K, Fekete G, Farkas Z, Lázár V, Hrtyan M, Kemmeren P,
685 Groot Koerkamp MJA, et al. 2014. The Genomic Landscape of Compensatory Evolution.Barton
686 NH, editor. PLoS Biol. 12:e1001935–16.

687 Taylor MB, Ehrenreich IM. 2015a. Transcriptional Derepression Uncovers Cryptic Higher-Order
688 Genetic Interactions.Wittkopp P, editor. PLoS Genet. 11:e1005606–e1005614.

689 Taylor MB, Ehrenreich IM. 2015b. Transcriptional Derepression Uncovers Cryptic Higher-Order
690 Genetic Interactions.Wittkopp P, editor. PLoS Genet. 11:e1005606–e1005614.

691 Thompson A, Zakon HH, Kirkpatrick M. 2015. Compensatory Drift and the Evolutionary Dynamics of
692 Dosage-Sensitive Duplicate Genes. Genetics:1–29.

693 True JR, Haag ES. 2001. Developmental system drift and flexibility in evolutionary trajectories. 3:109–
694 119.

695 Tsachaki M, Sprecher SG. 2011. Genetic and developmental mechanisms underlying the formation of
696 the Drosophila compound eye.Singh A, Irvine KD, editors. Dev. Dyn. 241:40–56.

697 Vincent L. 1993. Morphological grayscale reconstruction in image analysis: Applications and efficient
698 algorithms. IEEE transactions on image processing 2:176–201.

699 Ward LD, Kellis M. 2012. Interpreting noncoding genetic variation in complex traits and human
700 disease. Nat. Neurosci. 30:1095–1106.

701 Woodruff GC, Eke O, Baird SE, Felix M-A, Haag ES. 2010. Insights into species divergence and the
702 evolution of hermaphroditism from fertile interspecies hybrids of *Caenorhabditis* nematodes.
703 Genetics 186:997–1012.

704 Wunderlich Z, Bragdon MD, Eckenrode KB, Lydiard-Martin T, Pearl-Waserman S, DePace AH. 2012.
705 Dissecting sources of quantitative gene expression pattern divergence between Drosophila
706 species. Mol. Syst. Biol. 8:1–15.

707 Yassin A, Delaney EK, Reddieux A, Bastide H, Seher T, Appleton NC, Lack JB, David JR, Chenoweth
708 SF, Pool JE, et al. *pdm3* is responsible for recurrent evolution of female-limited color dimorphism
709 in *Drosophil*. Curr. Biol.

710